Journal of Power Sources 205 (2012) 151–156

Contents lists available at SciVerse ScienceDirect

Journal of Power Sources

journal homepage: www.elsevier.com/locate/jpowsour

Hysteresis controller based maximum power point tracking energy harvesting system for microbial fuel cells

Jae-Do Park[a,*], Zhiyong Ren[b]

[a] Department of Electrical Engineering, University of Colorado Denver, Denver, CO 80217, United States
[b] Department of Civil Engineering, University of Colorado Denver, Denver, CO 80217, United States

ARTICLE INFO

Article history:
Received 12 December 2011
Received in revised form 4 January 2012
Accepted 4 January 2012
Available online 12 January 2012

Keywords:
Microbial fuel cell (MFC)
Energy harvesting
DC/DC converter
Maximum power point tracking (MPPT)
Digital potentiometer

ABSTRACT

Microbial fuel cell (MFC) is a new approach to accomplish simultaneous waste treatment and alternative energy production. An MFC employs exoelectrogenic bacteria to directly convert biodegradable substrates to electricity. The electricity production from MFCs can be maximized at a certain operating condition, which is defined as the maximum power point (MPP). However, it is difficult to maintain an MFC at its MPP during operation, because the power output from MFCs fluctuates constantly due to the changes of microbial activities or environmental conditions. This study developed a maximum power point tracking (MPPT) technique using digitally controlled potentiometers for hysteresis controller based energy harvesting system. Results with lab scale MFC reactors have shown that the system can track the MPP and maintain the maximum energy harvesting in real-time, suggesting that the proposed system can capture the most available energy from MFCs at the most efficient operating point.

1. Introduction

Microbial fuel cell technology has been intensively researched in recent years as a novel technology, because it offers a solution for energy and environmental sustainability by simultaneously performing waste treatment and generating electricity – a clean, distributed, and even remote energy source. MFCs use electrochemically active bacteria to extract the electrons from biodegradable substrates in the anode chamber and transfer them to the anode electrode. These electrons flow from the anode through an external circuit to the cathode, where they reduce an electron acceptor such as oxygen or ferricyanide. The reported maximum power density from lab scale air-cathode reactors has been increased by orders of magnitude in the last few years, from less than 1 mW m^{-2} to 6.9 W m^{-2} [1,2]. The typical MFC power density measurement method involves operating the reactor with a static external resistance or applied potential, and then transiently obtaining polarization data by applying a series of different external resistances or performing an electrochemical scan using a potentiostat [3,4]. The maximum power density is achieved when the applied external resistance is equal to the MFC internal resistance [3–5]. Such characterizations represent the potential of MFC power output, but they don't measure the actually usable power output, because the generated electricity is dissipated into heat instead of being utilized by electronics. Moreover, the fixed resistance cannot recover the maximum power output during MFC operation, because the internal resistance of an MFC varies with changes in operational parameters, such as substrate concentration, pH, and temperature [6–8].

For efficient harvesting and usage of the MFC energy, technologies capable of real-time maximum power point tracking (MPPT) and the maximum available power capturing need to be developed. MFCs may lost more than 50% of produced power across the internal resistance if the operating voltage is not at the maximum power point (MPP) voltage [9]. In addition, compared to other physiochemical-reaction based processes, MFC performance depends on microbial activity, which is relatively slow and susceptible to many environmental condition changes such as instantaneous output power level, accumulated extracted energy, bacteria community and activity shifts. Furthermore, the output voltage of MFC does not remain constant as the current output increases, making the real-time energy tracking and capturing more challenging.

Popular MPPT techniques such as perturbation and observation (P&O) or gradient method for photovoltaic systems and hydrogen fuel cells were introduced to MFC systems for real-time optimal selection of the external resistance [5,9]. These techniques have been utilized to identify the value of proper external resistance to operate the MFC at MPP. However, finding the optimal external resistance still cannot capture and utilize the energy generated by MFCs. Another approach for harvesting system is using capacitor-based circuits such as super capacitors and charge pumps, which

* Corresponding author. Tel.: +1 303 352 3743; fax: +1 303 556 2383.
E-mail address: jaedo.park@ucdenver.edu (J.-D. Park).

0378-7753/$ – see front matter © 2012 Elsevier B.V. All rights reserved.
doi:10.1016/j.jpowsour.2012.01.053

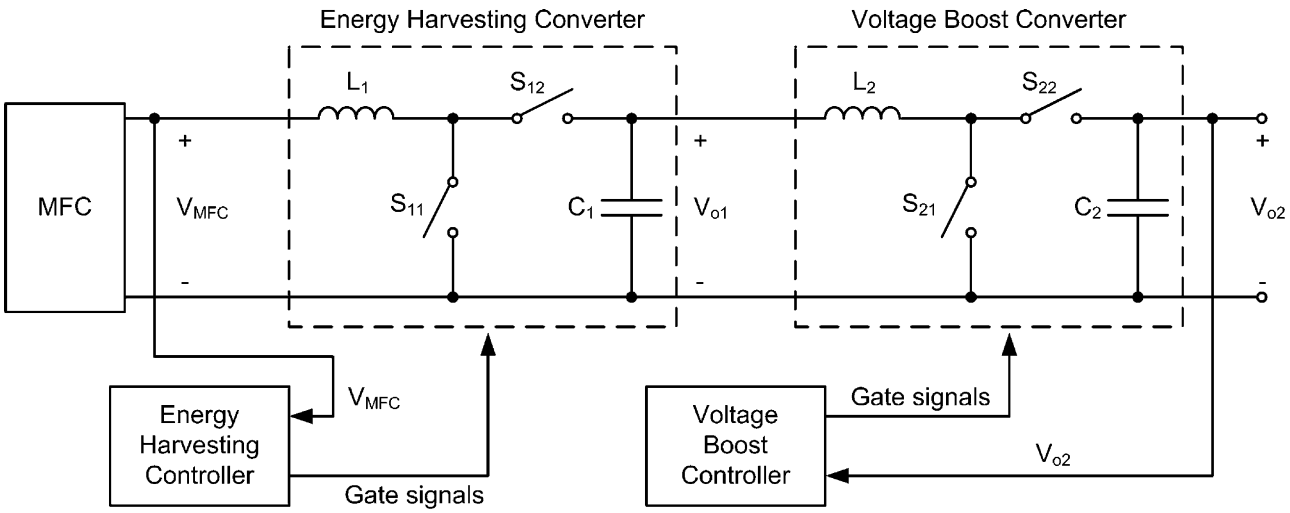

Fig. 1. Block diagram of hysteresis controller based MFC energy harvesting system.

capture the energy passively and transfer it to a boost converter [10–12]. But these systems are not suitable for MPPT either because of the limited controllability on operating condition.

In this study, an integrated control system that can perform both real-time MPPT and the maximum available power harvesting has been developed. The system does not utilize charge pumps and was operated under batch conditions with a hysteresis controller based energy harvesting system. The power output tracked and regulated by the controller was compared with the power generation from fixed external resistance operation, and the real-time parameter changing was compared with the polarization power curve.

2. Materials and methods

2.1. Hysteresis controller based MFC energy harvesting system

A hysteresis circuit based MFC energy harvesting system has been utilized in this paper. The energy harvester is the front-end of two layers of DC/DC converters: the first converter (energy harvester) captures the energy from an MFC, and the second layer converter (voltage booster) increases the voltage to a suitable level for the load. Fig. 1 shows the block diagram of the overall system, and operation details can be found in authors' previous work [13].

The system maintains the operating voltage at the MPP of MFC by switching the harvesting converter switches S_{11} and S_{12}. The operation of the energy harvester in the first layer consists of two modes, CHARGE and DISCHARGE: during CHARGE mode, the energy harvester's main switch S_{11} is turned on to get the energy extracted from the MFC and stored in the inductor L_1. The MFC voltage V_{MFC} decreases due to the increasing output current. This switch is off during the DISCHARGE mode, and the energy in the inductor L_1 is discharged to the storage capacitor C_1 through the secondary switch S_{12}. The MFC voltage recovers as current decreases. The switches are toggled complimentarily when the MFC voltage reaches lower threshold and upper threshold in the CHARGE and DISCHARGE mode, respectively. Generally, an N-channel MOSFET is utilized for S_{11} because of high switching speed and low conduction loss. For S_{12}, a diode can be used for simple circuit configuration, but it suffers from high forward voltage drop. For better efficiency, a synchronous converter can be implemented using a P-channel MOSFET as S_{12}, but it requires a complex gate drive circuitry because it is a floating switch. The upper and lower voltage thresholds are given as $V_{thH} = V_{CC} \cdot R_2/\{R_2 + (R_1//R_3)\}$ and $V_{thL} = V_{CC} \cdot (R_2//R_3)/\{R_1 + (R_2//R_3)\}$. The frequency of power extraction, i.e., the transition between CHARGE and DISCHARGE mode, is automatically controlled according to the MFC's condition so that the MFC voltage can be confined in a pre-defined voltage band, $V_{thH} - V_{thL}$, and at the same time enough recovery time of the MFC reactor is ensured. This scheme is especially effective for the weak MFC units which experience significant internal voltage drop with an output current increase. The second layer with a standard DC/DC boost converter increases the output voltage to

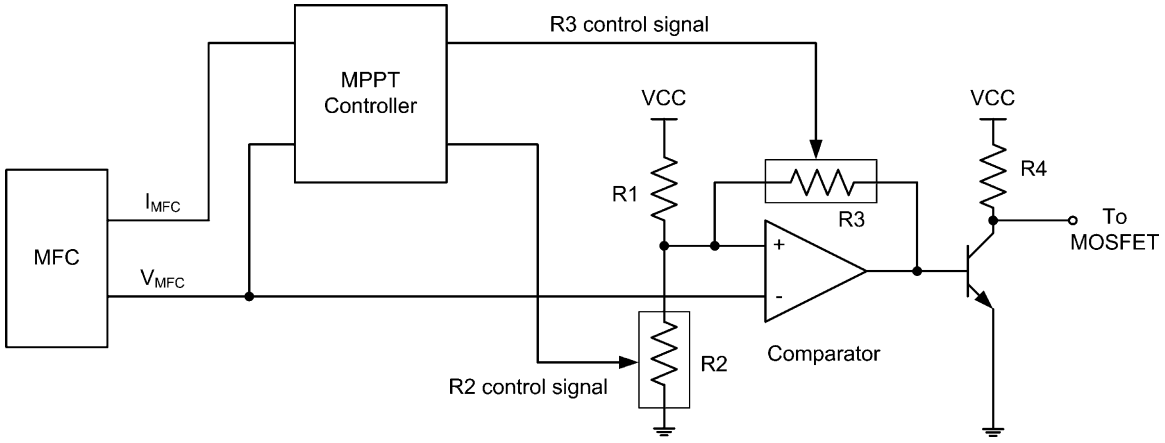

Fig. 2. Proposed MPPT controller using digital potentiometers.

a practically usable level, but it can be optional if the load takes burst-type power.

2.2. Hysteresis controller based maximum power tracking and harvesting

In order to track and maintain the operating point at MPP continuously despite the conditions (and therefore polarization curve) changing during MFC operation, digitally controllable potentiometers have been integrated into the hysteresis-based energy harvester (Fig. 2). The MFC voltage and current outputs are monitored and fed into the MPPT controller for instantaneous output power calculation. Then the MPPT controller generates control signals for R_2 and R_3 to adjust the operating voltage based on the calculated power. A reduced degree-of-freedom control scheme was created for the hysteresis controller to overcome the coupling problem of the multiple resisters. The system controls the voltage thresholds and hysteresis band based only on R_2. The feedback resistor R_3 is adjusted as a function of R_2.

The upper and lower voltage thresholds can be written as

$$V_{thH} = V_{CC} \cdot \frac{R_1R_2 + R_2R_3}{R_1R_2 + R_2R_3 + R_1R_3} \quad (1)$$

$$V_{thL} = V_{CC} \cdot \frac{R_2R_3}{R_1R_2 + R_2R_3 + R_1R_3}. \quad (2)$$

If R_3 is adjusted as a dependent variable of R_2, such as $R_3 = K \cdot R_2$, the thresholds can be given as follows.

$$V_{thH} = V_{CC} \cdot \frac{R_1 + KR_2}{(K+1)R_1 + KR_2} \quad (3)$$

$$V_{thL} = V_{CC} \cdot \frac{KR_2}{(K+1)R_1 + KR_2} \approx V_{CC} \cdot \frac{R_2}{R_1 + R_2} \quad (4)$$

Then the hysteresis voltage band becomes

$$V_{\text{band}} = V_{CC} \cdot \frac{R_1}{(K+1)R_1 + KR_2} \approx V_{CC} \cdot \frac{1}{K} \cdot \frac{R_2}{R_1 + R_2}. \quad (5)$$

It has been shown in (3) that the lower threshold can now be controlled with fixed R_1 and variable R_2, and the coefficient K determines the hysteresis voltage band with given R_1 and R_2 in (5). Although the hysteresis voltage band varies as the voltage thresholds change, it can be maintained reasonably small by using a simple linear coefficient, such as $K = C\{1 - R_2/R_1\}$, where C is a constant. For example, the hysteresis voltage band will be 18–20 mV if $C = 50$ and 1.5 V reference voltage.

For the experiment in this paper, the P&O method was implemented. A discrete-domain equation for R_2 adjustment based on P&O technique can be given as follows, where P_o is the calculated output power and K_R is the adjustment gain to control the step size.

$$R_2[n+1] = R_2[n] + K_R \frac{P_o[n] - P_o[n-1]}{R_2[n] - R_2[n-1]} \quad (6)$$

The controller adjusts R_2 in the direction that increases the output power and finds the instantaneous MPP.

3. Experimental

3.1. MPPT controller

For MPP tracking, the MPPT controller block in Fig. 2 has been implemented using digitally controllable potentiometers. Microchip MCP4251 5 kΩ and 100 kΩ has been chosen for R_2 and R_3, respectively. Each MCP4251 has two potentiometer channels and for R_3, they are connected in series to double the resistance range. MCP4251s are controlled using serial peripheral interface (SPI) bus from TI 320F28335 Digital Signal Processor (DSP) control

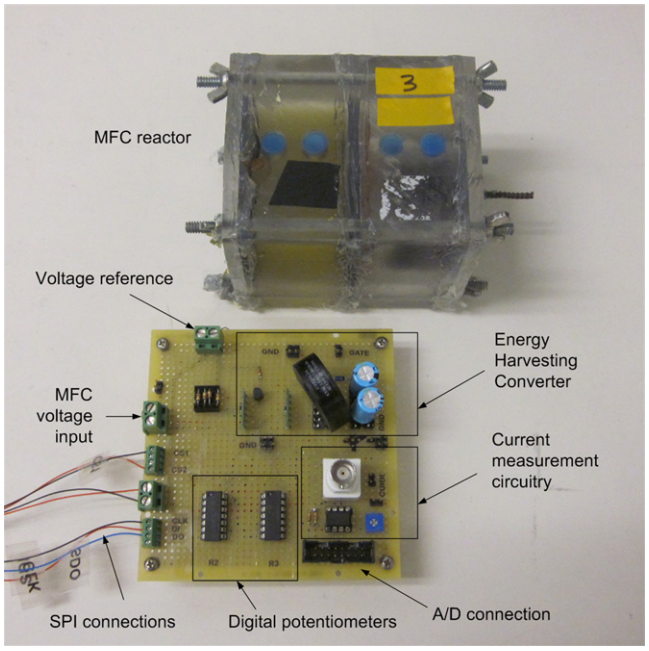

Fig. 3. MPPT experiment setup.

board. The voltage and current measurement and power calculation routines, and resistance control algorithm have been implemented in DSP firmware. In this experiment, R_2 and R_3 were adjusted as follows:

$$\Delta R_2 = sgn(\Delta P_o \times \Delta R_{2o}) \frac{5\ \text{k}\Omega}{N_{\text{step}}} \quad (7)$$

$$R_2[n+1] = R_2[n] + \Delta R_2 \quad (8)$$

$$R_3[n+1] = 50 \cdot \left(1 - \frac{R_2[n+1]}{R_1}\right) \cdot R_2[n+1] \quad (9)$$

where, $\Delta P_o = P_o[n] - P_o[n-1]$, $\Delta R_{2o} = R_2[n] - R_2[n-1]$ and sgn(x) function returns the polarity of x. A fixed resistance step and unity adjustment gain was used in this experiment. The N_{step} is the maximum number of the digital potentiometer steps. MCP4251 has 257 steps, which makes the R_2 step size 19.45 Ω. The R_2 has been adjusted one step size up or down according to the polarity of $\Delta P_o \times \Delta R_{2o}$ at every control interval.

To calculate the instantaneous power P_o, the MFC output current has been measured using Tektronics A622 current probe and fed into the DSP A/D converter as well as the MFC voltage. Due to the

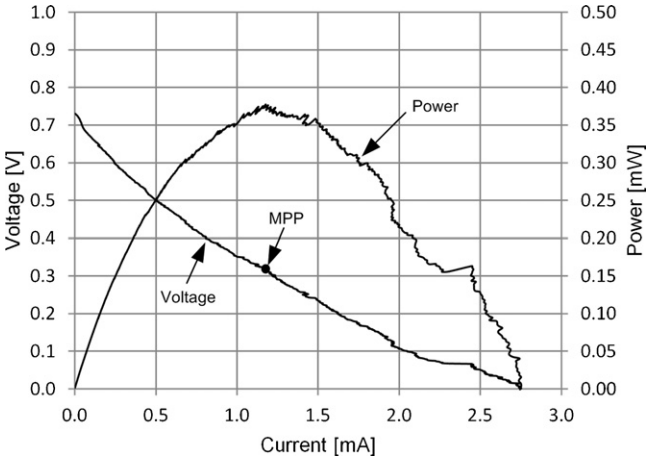

Fig. 4. Polarization curve of MFC.

very low output current level, a 100-turn coil and a non-inverting amplifier with ×21 gain has been used for current measurement. The output voltage boost converter in second layer of Fig. 1 was omitted in this MPPT experiment. The MPPT capable energy harvesting converter and the MFC reactor used in the experiment are shown in Fig. 3.

3.2. MFC reactor and operation

Two-chamber cubic-shaped MFC reactor was constructed and the diameter of each chamber was 7 cm [11]. The anode and cathode chambers were separated by a cation exchange membrane (CEM, CMI 7000, Membranes international, NJ) and the volume of each chamber was 140 mL. Heat treated graphite brushes were used as the anodes, and plain carbon paper was selected as the cathode material [14]. Phosphate (50 mM) buffered ferricyanide was used at the catholyte to minimize the cathode effects on system performance. After inserting the electrodes, the volume of each chamber was approximately 140 mL. Reactors were inoculated using effluent from another MFC operated in the same lab for more than one year. Anolyte medium solution was prepared containing 1.25 g L^{-1} CH_3COONa, 0.31 g L^{-1} NH_4Cl, 0.13 g L^{-1} KCl, 3.321 g L^{-1} $NaH_2PO_4{\cdot}2H_2O$, 10.317 g L^{-1} $Na_2HPO_4{\cdot}12H_2O$, 12.5 mL L^{-1} mineral solution, and 5 mL L^{-1} vitamin [15,16]. Reactors were operated in fed-batch mode at room temperature and refilled with new medium solution as required by electrical characterization. Polarization test was performed by a potentiostat (Gamry Instruments, PA, USA) at a scan rate of 0.1 mV s^{-1}, and the power curve and MPP can be seen in Fig. 4.

4. Results and discussion

Fig. 5 clearly shows the real-time operating point control and tracking of the MPP on the polarization curve of MFC under test. The controlled operating voltage and power density (bold) follows the polarization curve until it reaches the MPP. It can be seen in Fig. 6 that the proposed system tracks the MPP that is changing

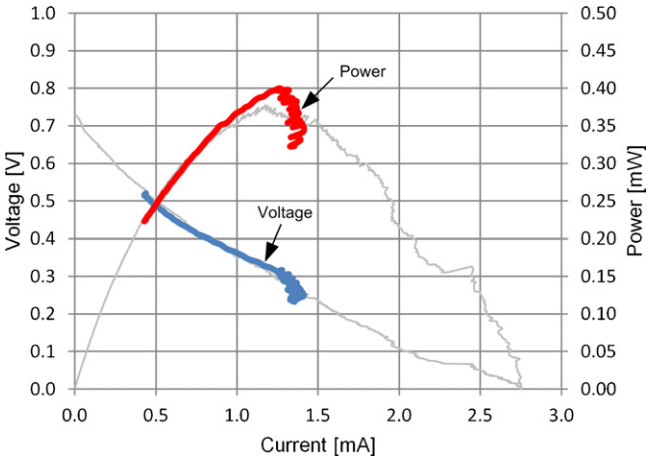

Fig. 5. MPPT control experiment result on polarization curve.

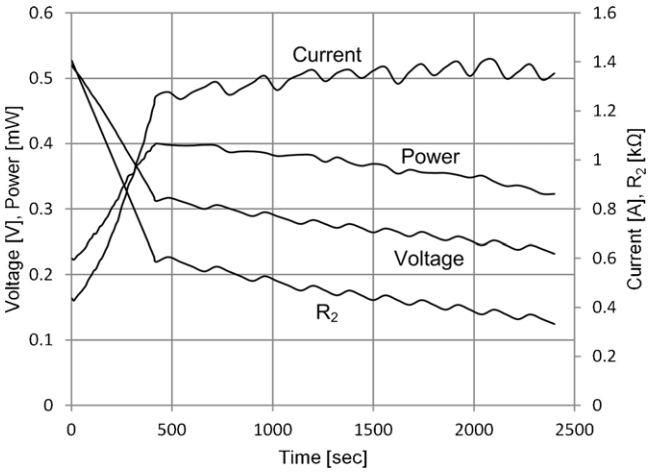

Fig. 6. MPPT control experimental result on time axis.

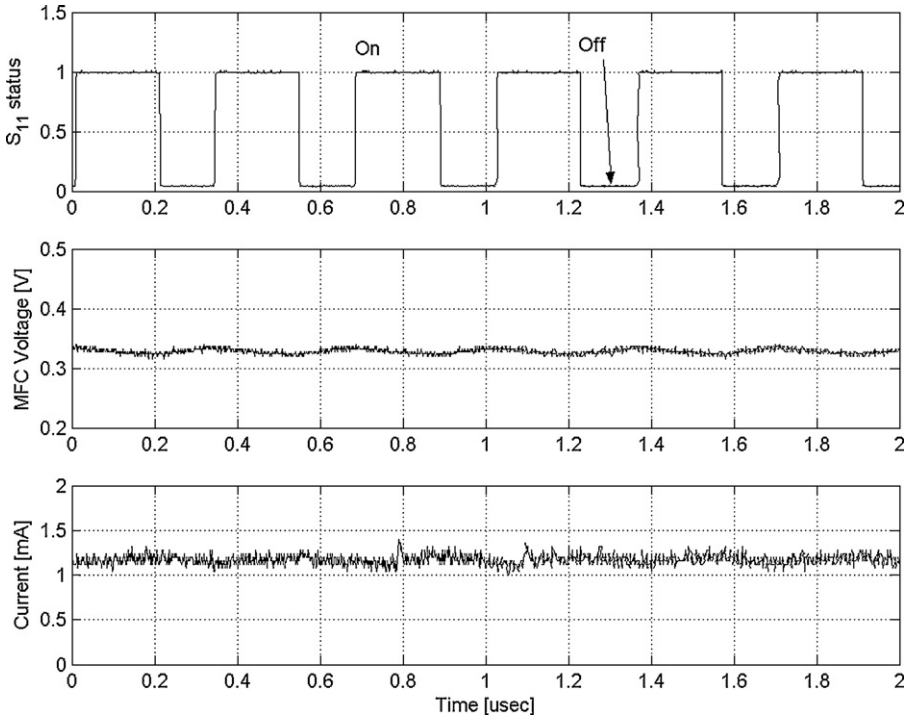

Fig. 7. Detailed operation of energy harvesting controller. Top: on/off status of switch S_{11}. Middle: MFC voltage. Bottom: MFC current.

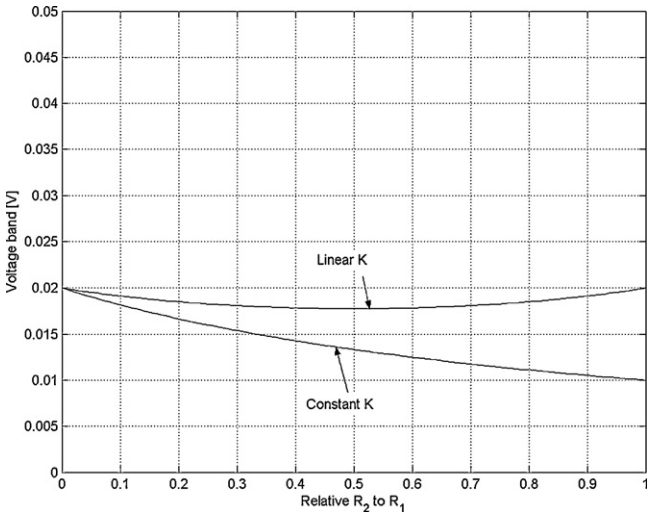

Fig. 8. Width of the hysteresis voltage band of constant coefficient $K = 50$ and linear coefficient $K = 50\{1 - 0.5(R_2/R_1)\}$.

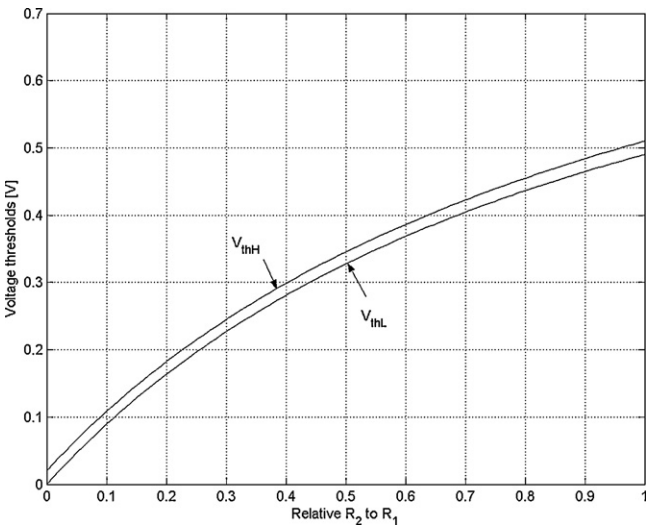

Fig. 9. Operating voltage thresholds according to R_2 variation. The horizontal axis denotes relative R_2 resistance to R_1. A 1.5 V voltage reference and $K = 50\{1 - 0.5(R_2/R_1)\}$ is used.

over time, which has the result of MPPT control experiment plotted on time axis. The MPPT algorithm was activated when the MFC voltage is 0.52 V at time zero and adjusted R_2 at every 10 s until the output power changes its direction. Then the power calculation and resistance adjustment interval was increased to 60 s. The controller found the MPP at around 0.32 V at around 460 s, and maintained the operating point at the changing MPP afterwards by adjusting operating voltage. It can also be seen that the output current is maintained at a constant level but the voltage and power droop as the MFC generates power continuously. An example of detailed operation of the harvesting controller is shown in Fig. 7. The top waveform shows the on/off status of switch S_{11}. The system is in CHARGE and DISCHARGE mode when the switch is on and off, respectively. It can be seen that the MFC voltage is increased and decreased in each mode in second waveform. At this particular instance, the MFC output voltage is controlled at around 320 mV. The MFC current is shown in the last waveform.

Unlike many abiotic power systems whose power output is considered constant due to stable physical or chemical reactions, the output power of the MFC reactor is determined by the dynamic microbial activity in the anode chamber. The bacterial community and activity vary constantly due to the changes of microbial metabolism and environmental conditions such as pH, temperature, or substrate concentration, so the associated power production changes accordingly. Such variations can be minimized by optimizing microbial growth conditions through system operation to stabilize environmental factors, but the stabilization of microbial activity generally takes hours or longer. Such characteristics are reflected in the voltage waveform in Fig. 6, where the voltage declined gradually due to the slow response of microbial activity. Substrate depletion in batch operation may also cause gradual voltage decline, and continuous flow operation will be further conducted to avoid such effects. To our best knowledge, no control system has been reported that is able to track the MPP *in situ* while capturing actually usable energy from such microbial systems.

As can be seen in (5), the hysteresis voltage band is a function of resistances R_1, R_2 and coefficient K. Although the control is simplified by decreasing the degree-of-freedom, the width of the hysteresis band varies as the ratio of R_2 to R_1 changes. If a constant value C is used for K over the zero to one range of R_2 to R_1 ratio, the initial voltage band when $R_2 = 0$ is given as $1/C$ V and the maximum voltage band deviation is almost 50% when $R_2/R_1 = 1$. This can result in inconsistent operational conditions. This band width variation can be reduced with variable coefficient K. If K changes linearly as a function of the resistance ratio, such as $K = C\{1 - 0.5(R_2/R_1)\}$, the maximum variation of the band width is reduced to about 11%, so that the reasonably constant operating condition can be maintained over a wide voltage range. In Fig. 8, the hysteresis voltage band by the constant coefficient $K = C = 50$ and linear coefficient $K = 50\{1 - 0.5(R_2/R_1)\}$ are shown. It can be seen that the hysteresis voltage band variation with linear coefficient K is significantly smaller compared to the one with the constant coefficient K. Fig. 9 shows the upper and lower voltage threshold with linear coefficient $K = 50\{1 - 0.5(R_2/R_1)\}$.

A general DSP microcontroller board has been utilized for this experiment and the power for the control circuit has been supplied from an external power supply. It is because the controller is not designed for the low-power application and the minimal power consuming control circuit design has not been investigated in this paper. However, using low power parts and a CMOS ASIC would be a feasible approach for minimal power consuming control circuit implementation and self-sustainability.

5. Conclusions

In this paper, a hysteresis controller based MFC energy harvesting system that is capable of maximum power point tracking and maximum available energy harvesting has been developed using digitally controlled potentiometers for the first time. Compared to the traditional systems, the proposed system eliminated external resistances and enabled simultaneous MPP tracking and maximum MFC energy capture in real-time. This approach provides a new way of robust and efficient MFC operation for maximizing output power and carries potential to significantly advance the development and application of microbial fuel cell technology.

Acknowledgements

This work was supported by University of Colorado Denver College of Engineering and Applied Science (Park) and the Office of Naval Research (ONR) under Award N000140910944 (Ren). Authors thank Dr. Haiping Luo for providing the MFC reactors.

References

[1] B. Min, S. Cheng, B.E. Logan, Water Res. 39 (2005) 1675–1686.
[2] B.E. Logan, Appl. Microbiol. Biotechnol. 85 (2010) 1665–1671.
[3] Z. Ren, H. Yan, W. Wang, M. Mench, J. Regan, Environ. Sci. Technol. 45 (2011) 2435–2441.
[4] K.S. Jacobson, D.M. Drew, Z. He, Bioresour. Technol. 102 (2011) 376–380.
[5] R.P. Pinto, B. Srinivasan, S.R. Guiot, B. Tartakovsky, Water Res. 45 (2011) 1571–1578.
[6] H. Liu, S. Cheng, B.E. Logan, Environ. Sci. Technol. 39 (2005) 658–662.
[7] G.C. Gil, I.S. Chang, B.H. Kim, M. Kim, J.K. Jang, H.S. Park, H.J. Kim, Biosens. Bioelectron. 18 (2003) 327–334.
[8] S.A. Cheng, D.F. Xing, B.E. Logan, Biosens. Bioelectron. 26 (2011) 1913–1917.
[9] L. Woodward, M. Perrier, B. Srinivasan, R.P. Pinto, B. Tartakovsky, AIChE J. 56 (2010) 2742–2750.
[10] C. Donovan, A. Dewan, H. Peng, D. Heo, H. Beyenal, J. Power Sources 196 (2011) 1171–1177.
[11] F. Zhang, L. Tian, Z. He, J. Power Sources 196 (2011) 9568–9673.
[12] A. Meehan, G. Hongwei, Z. Lewandowski, IEEE Trans. Power Electron. 26 (2011) 176–181.
[13] J. Park, Z. Ren, Proceedings of IEEE Energy Conversion Congress and Exposition, 2011, pp. 3852–3858.
[14] H. Wang, Z. Wu, A. Plaseied, P. Jenkins, L. Simpson, C. Engtrakul, Z. Ren, J. Power Sources 196 (2011) 7465–7469.
[15] H. Luo, P.E. Jenkins, Z. Ren, Environ. Sci. Technol. 45 (2011) 340–344.
[16] H.M. Wang, M. Davidson, Y. Zuo, Z.Y. Ren, J. Power Sources 196 (2011) 5863–5866.